



RESEARCH ARTICLE

Instability of isolator shocks to fuel flow rate modulations in a strut-stabilised scramjet combustor

R. Kumar  and A. Ghosh 

Department of Aerospace Engineering, Indian Institute of Technology, Kharagpur, West Bengal, India

Corresponding author: R. Kumar; Email: rajesh.kumar@iitkgp.ac.in

Received: 4 March 2024; **Revised:** 5 August 2024; **Accepted:** 23 September 2024

Keywords: mode transition; thermal choking; dual-mode scramjet; strut; supersonic; shockwaves

Abstract

Reynolds-Averaged Navier–Stokes (RANS) simulations, both steady and unsteady, are used to investigate supersonic, chemically reacting, flow fields inside a strut-stabilised supersonic combustion ramjet (scramjet) engine operating under different fuel flow rates. Fully supersonic, fully subsonic and mixed modes of operations inside the combustor, obtained at different fuel flow rates, are studied numerically through shock wave visualisations and top-wall static-pressure probing. The effect of changing fuel flow rates, imposed both suddenly and gradually, on the behaviour of shock waves and wall pressure profiles are studied in detail. For certain modes of combustion characterised by the presence of oblique shocks at the strut, shockwaves in the combustor respond predictably to an increase or decrease in fuel flow rate attaining the steady state flow fields as predicted by RANS simulations for those fuel flow rates. For certain other modes of combustion, characterised by the presence of shockwaves in the isolator and the absence of oblique shocks at the leading edge of the strut, shockwaves in the flow field appear unstable to fuel flow rate modulations. For such cases, any change in fuel flow rates, sudden or gradual, increase or decrease, causes the isolator shocks to immediately move upstream and eventually out of the isolator. A plausible physics-based explanation of the observed phenomena is presented.

Nomenclature

M	Mach number
H	total enthalpy
T_t	total temperature
T_i	static temperature at the inlet
u_i	velocity components
PR	ratio of static pressure at fuel inlet to air inlet
Φ	equivalence ratio
$\dot{m}_{i,air}$	mass flow rate of vitiated air(gm/s)

Symbols

γ	specific heat ratio
----------	---------------------

Subscripts

i	inlet
-----	-------

1.0 Introduction

Among the various challenges associated with scramjet engines, the loss of stagnation pressure resulting from heat addition under supersonic flow conditions, the competition between ignition-delay and flow-residence timescales, the reduction in shear layer mixing due to compressibility effects, and the sudden transition between supersonic and subsonic modes of operation resulting from thermal choking are considered most critical [1–3]. Mode transition, in particular, can cause sudden changes in mechanical and thermal loads experienced by the combustor and can cause sudden changes in thrust levels generated by the engine. The problem of mode transition has become a focal point of technological interest, more so, given the potential of the scramjet engine in expanding the operational envelope of air-breathing engines and other combined cycle configurations [4, 5].

The RAM-SCRAM mode transition, typically triggered by an increase in inflow Mach number due to vehicle acceleration or due to a reduction in equivalence ratio, has been a subject of study for an extended period, initially demonstrated experimentally by Billig [8]. Building on Billig's research, Sullins [9] conducted experimental investigations into the transition from a dual-mode to a purely scramjet mode. Acceleration from $M=5.9$ to 6.2 while maintaining a constant fuel/air equivalence ratio was studied. Fotia et al. [10–12] studied RAM-SCRAM transition behaviours under various conditions contributing to a better understanding of the factors influencing the initiation and sustenance of the mode transition process. The reverse problem of SCRAM-RAM mode transition and the subsequent phenomena of flame flashback [13] and inlet unstart [22–24], often associated with such transitions, have also been studied both experimentally [9, 11, 14–27] and computationally [28–33]. Increase in fuel mass flow rates [34, 42], changes in combustor geometry or combustor configurations [35], rise in combustion chamber pressure have all been shown to induce SCRAM-RAM transitions under controlled conditions.

The current work utilises two dimensional (2D) RANS/URANS simulations to study mode transitions in the German Aerospace Center's (DLR), single-strut, parallel-flow, dual-mode scramjet (DMSJ) combustor and reports an interesting case of instability of isolator shocks under certain modes of operation. The commercially available Ansys Fluent software is used to obtain spatio-temporally resolved wall pressure data and shock-train visualisations in the combustor and the isolator under various modes of operation (fully supersonic, partly supersonic and fully subsonic) for both fixed and temporally varying fuel flow rates. Mach numbers at the air and fuel inlets are held constant at 1.7 and 1.0, respectively. Fuel-air inlet pressure ratio 'PR' is used as a parameter. Holding the static pressure at the vitiated air inlet constant throughout the study, a change in pressure ratio (PR) is effected by changing the static pressure at the sonic gaseous hydrogen (GH₂) fuel inlet. Higher PRs mean higher fuel flow rates, hence higher heating rates. Lower PRs mean lower fuel flow rates, hence lower heating rates.

For SCRAM modes of combustion occurring at low fuel flow rates characterised by oblique shock waves at the leading edge of the strut but no shock waves in the isolator, shockwaves in the combustor are shown to respond predictably to an increase or decrease in fuel flow rates attaining the steady state flow fields as predicted by RANS simulations at those fuel flow rates. For RAM modes of combustion occurring at relatively higher fuel flow rates characterised by shockwaves in the isolator but no oblique shocks at the leading edge of the strut, shockwaves in the isolator are shown to be unstable to fuel flow rate modulations. Any change in fuel flow rate, increase or decrease, sudden or gradual is shown to cause the isolator shocks to immediately move upstream leading to unstart like conditions rendering the entire flow field subsonic. Our simulations indicate that modes with oblique shock at the strut are not realisable through a reduction in fuel flow rate alone once a mode of the later type is established. Section 4.2.2 describes this phenomenon. Section 4.3 provides a plausible physical explanation for this phenomenon.

2.0 Technical background

The Rayleigh-Flow formulation provides a quasi-1D model for capturing the effects of heat addition to a subsonic or supersonic flow [1]. As per this model, heat added to a supersonic flow increases static

Table 1. Grid densities

Boundary information	Number of divisions
Air inlet	400
Fuel inlet	10
Exit	460
Bottom wall	1360
Strut walls (inclined)	128
Strut wall (near injector)	25

Table 2. Air and fuel inlet conditions

Propellant	Inflow parameters	Case						
		1	2	3	4	5	6	7
Oxidizer: vitiated air 23% O_2 3.2% H_2O 73.8% N_2 by mass	M_i	1.7	1.7	1.7	1.7	1.7	1.7	1.7
	T_i (K)	570	570	570	570	570	570	570
	P_i (atm)	1.46	1.46	1.46	1.46	1.46	1.46	1.46
	$\dot{m}_{i,air}$ (gm/s)	35.99	35.99	35.99	35.99	35.99	35.99	35.99
	\dot{m}_{i,O_2} (gm/s)	8.28	8.28	8.28	8.28	8.28	8.28	8.28
	M_i	1.0	1.0	1.0	1.0	1.0	1.0	1.0
	T_i (K)	300	300	300	300	300	300	300
Fuel: H_2	P_i (atm)	2.92	10.22	14.6	15.33	16.06	16.79	17.52
	\dot{m}_{i,H_2} (gm/s)	0.31	1.10	1.57	1.65	1.73	1.81	1.89
	PR	2	7	10	10.5	11	11.5	12
	Φ	0.29	1.04	1.49	1.56	1.64	1.71	1.78

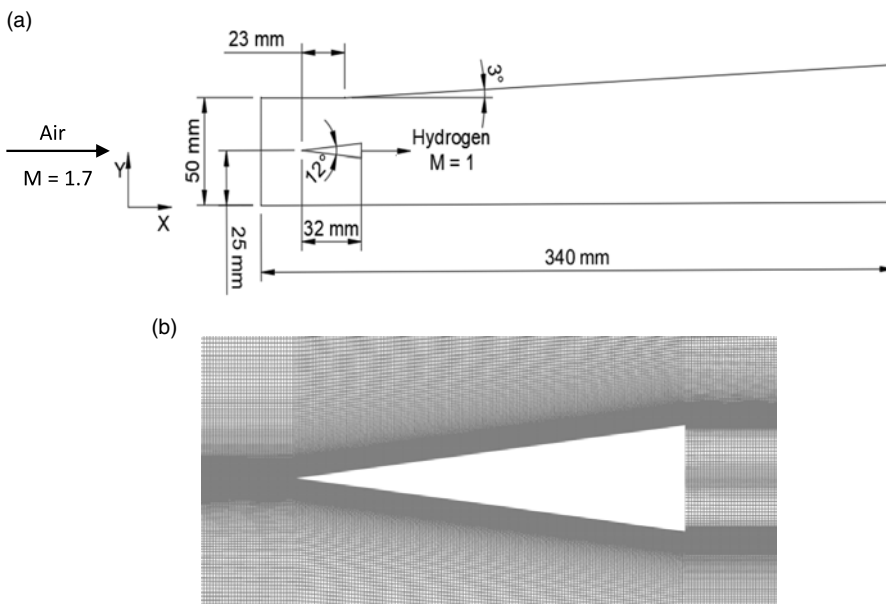


Figure 1. 2D computational details of DLR geometry (a) Dimensions (b) Grid.

Table 3. Test conditions

Run	Flow	Simulation	Solution	ΔPR	Initial	Final	Δt (ms)
1	Non-reacting	Steady	RANS	None	2	2	
2	Non-reacting	Steady	RANS	None	7	7	
3	Non-reacting	Steady	RANS	None	10	10	
4	Non-reacting	Steady	RANS	None	10.5	10.5	
5	Non-reacting	Steady	RANS	None	11	11	
6	Non-reacting	Steady	RANS	None	11.5	11.5	
7	Non-reacting	Steady	RANS	None	12	12	
8	Reacting	Steady	RANS	None	2	2	
9	Reacting	Steady	RANS	None	7	7	
10	Reacting	Steady	RANS	None	10	10	
11	Reacting	Steady	RANS	None	10.5	10.5	
12	Reacting	Steady	RANS	None	11	11	
13	Reacting	Steady	RANS	None	11.5	11.5	
14	Reacting	Steady	RANS	None	12	12	
15	Reacting	Transient	URANS	None	7	7	
16	Reacting	Transient	URANS	Step increase	7	12	
17	Reacting	Transient	URANS	Step increase	10	12	
18	Reacting	Transient	URANS	Step decrease	12	10	
19	Reacting	Transient	URANS	Step decrease	11.5	7	
20	Reacting	Transient	URANS	Step decrease	11	7	
21	Reacting	Transient	URANS	Step increase	7	11.5	
22	Reacting	Transient	URANS	Step increase	7	12	
23	Reacting	Transient	URANS	Ramped increase	10	12	10
24	Reacting	Transient	URANS	Ramped decrease	12	10	10
25	Reacting	Transient	URANS	Ramped decrease	11	7	10
26	Reacting	Transient	URANS	Step increase	11	11.5	
27	Reacting	Transient	URANS	Step increase	2	7	
28	Reacting	Transient	URANS	Step increase	7	10	
29	Reacting	Transient	URANS	Step decrease	11	10.5	

pressure, reduces Mach number, eventually causing the flow to thermally choke. Upon further addition of heat, the supersonic flow abruptly transitions into a subsonic flow across a normal shockwave. This transition causes an increase in the area under the TS curve accommodating an amount of heat that is greater than that required for thermal choking. Shapiro [1] extends this quasi-1D model by incorporating the presence of area change, friction and mass addition. Equation (1) describes the variation in Mach number and the possibility of choking under the combined effects of area change, friction and heat addition and indicates why an increase in cross sectional area is often employed in supersonic combustors to delay or prevent thermal choking due to heat addition.

$$\frac{1 - M^2}{2(1 + \frac{\gamma-1}{2}M^2)} \frac{dM^2}{M^2} = \frac{-dA}{A} + \frac{\gamma M^2}{2} \frac{4C_f dx}{D} + \frac{1 + \gamma M^2}{2} \frac{dT_t}{T_t} \quad (1)$$

$$\frac{1}{P} \frac{dP}{dx} = \frac{\gamma M^2}{1 - M^2} \frac{1}{A} \frac{dA}{dx} - \frac{\gamma M^2(1 + \frac{\gamma-1}{2}M^2)}{1 - M^2} \frac{1}{T_t} \frac{dT_t}{dx} \quad (2)$$

While the quasi-1D model gives a simplified tool for interpreting flow with heat addition, in practical engines, because of the preponderance of oblique shocks, shock-boundary-layer interactions,

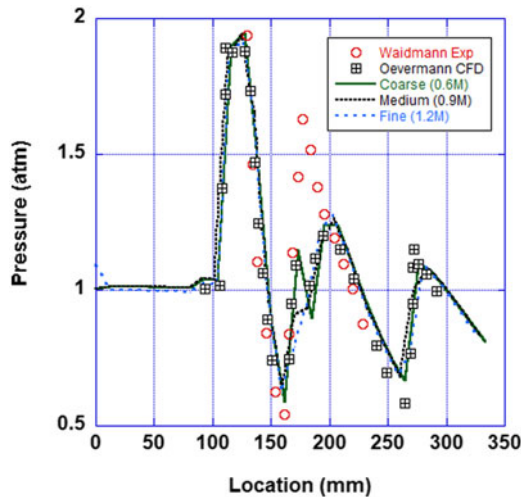


Figure 2. Code validation: lower wall pressure (non-reacting flow).

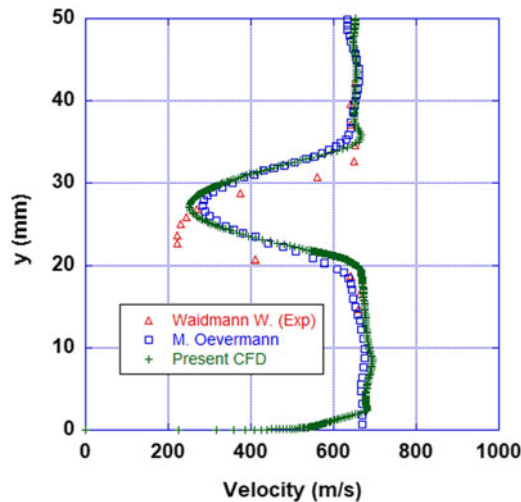


Figure 3. Code validation: velocity ($x = 125\text{mm}$, reacting flow).

shock-shear-layer interactions, the flow field no longer remains quasi-1D. Experimental or numerical methods therefore become necessary to predict shock activities in the combustor and in the isolator under varying heat loads. In DMSJ engines, the SCRAM mode typically exhibits a series of oblique shockwaves that steepen upon increased heat addition. The steepening of the oblique waves in the combustor is primarily to match the increased static pressure in the supersonic stream due to higher heat loads. Eventually, part of the combustor may turn subsonic, presenting itself as a flow-field devoid of shock activities. Isolator shocks may also steepen or move upstream depending on the downstream pressure the flow has to accommodate. In extreme cases, the shocks in the isolator may be pushed further upstream causing the inlet to unstart.

Equation (2) shows the variation in static pressure along the flow due to the variation of both cross sectional area and total temperature. If constant area is considered, static pressure would rise in a supersonic flow with heat addition while it would decrease for a subsonic flow with heat addition. For interpreting

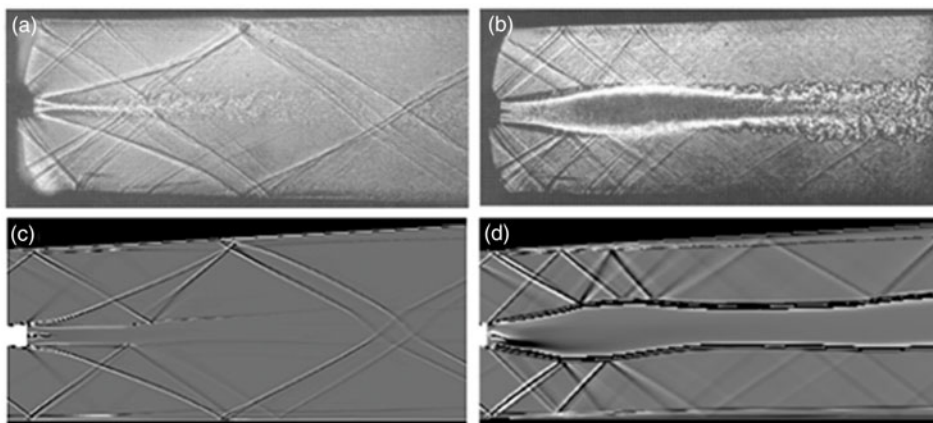


Figure 4. Experimentally obtained shadowgraph image [33] (a) Non-reacting (b) Reacting. Numerically obtained shadowgraph image (c) Non-reacting (d) Reacting.

the variation in wall pressure in the combustor under SCRAM or RAM modes of operation, the variation in area of the relevant stream tube and heat addition both need to be considered.

3.0 Computational methodology

Figure 1a shows the computational domain for the 2D strut-based DMSJ combustor used in this work. The model is based on the German Aerospace Center's (DLR), 2D single-strut, parallel-flow, dual-mode scramjet (DMSJ) combustor [33]. The left bottom corner represents the (0,0) coordinate. Pointwise software is used for grid generation. Ansys-Fluent is used for numerical simulations. Table 1 shows grid densities at different regions of the model. Grid density near the strut is shown in Fig. 1b. The flow equations are solved on a grid with 6,05,234 cells using an implicit density-based solver.

Solver settings, chemistry model, justifications for using the $k - \omega$ SST model [37, 38] are discussed in our previous papers [39, 40]. The single-step reaction, $2H_2 + O_2 \rightarrow 2H_2O$, is used with the Arrhenius reaction rate equation $K_f = AT^\beta \exp\left(-\frac{E}{RT}\right)$ where A = pre-exponential factor (consistent units), T = temperature (K), β = temperature exponent (dimensionless), E = activation energy for the reaction (J/kg.mol), and R = Universal gas constant (J/kg.mol.K). A finite rate/eddy dissipation model has been used for the hydrogen and vitiated air mixture. Previous numerical studies involving hydrogen-air [6] and hydrogen-oxygen [7] combustion have shown good agreement between single step and multi-step chemistry in the prediction of product formation and flow field features in supersonic flows [6, 7] justifying the use of the single step in the current work.

Boundary conditions used in this study are shown in Table 2. Various tests performed in this study are shown in Table 3.

Figure 2 shows lower-wall pressure distribution obtained using three different meshes, Mesh1 (0.6 million cells), Mesh2 (0.9 million cells) and Mesh3 (1.2 million cells) along with previously reported results from experimental and numerical studies [33]. Fig. 3 compares the x-velocities at different y locations at $x = 125$ mm. Reasonable agreement with the original experimental works of Waidmann and the widely used computational results of Oevermann can be observed [33]. Mesh1 is used for all results reported in this work. Figures 4a and 4b show experimentally obtained shadowgraph images of the cold and reacting flow tests performed by Waidmann [33]. Figures 4c and 4d show numerically obtained shadowgraph images of the cold flow and reacting flow respectively from the present study. Results are seen to agree qualitatively with Waidmann's experiments.

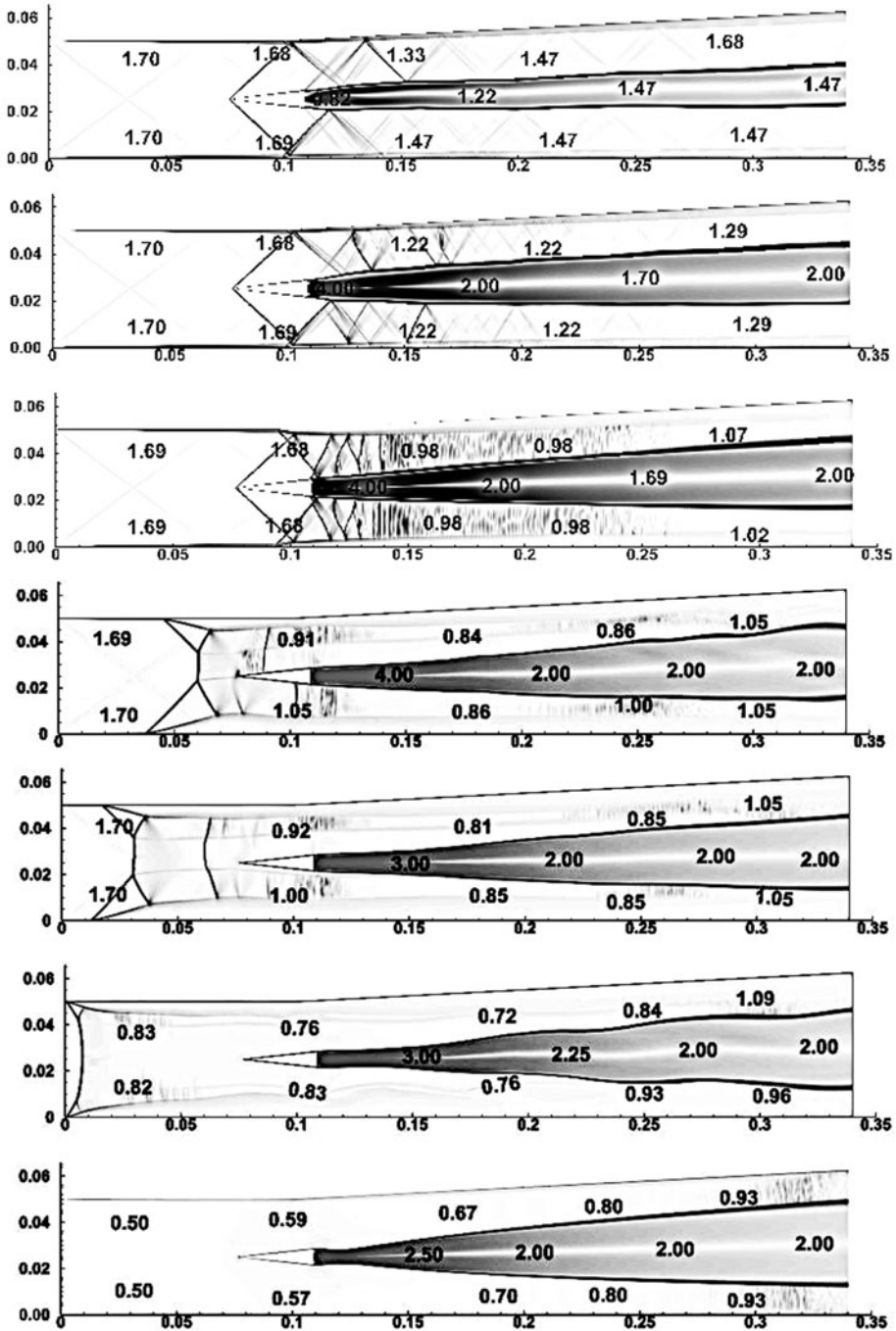


Figure 5. Numerical schlieren images for reacting flowfields obtained using RANS at different fuel flow rates. From top to bottom, $PR = 2, 7, 10, 10.5, 11, 11.5$ and 12 . Mach numbers superimposed.

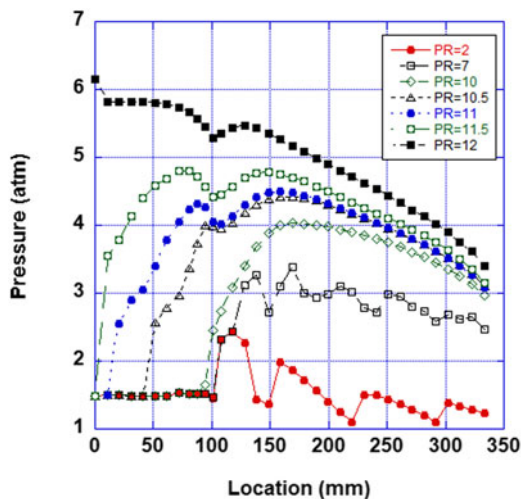


Figure 6. Top wall pressure distribution (reacting flow).

4.0 Results and discussions

4.1 Steady-state behaviour

RANS (SST $k-\omega$) simulations are used to obtain steady state behaviour of shock waves (Fig. 5) for reacting flow conditions in a strut-stabilised dual-mode SCRAMJET combustor revealing different modes of combustion under different PRs. Image axes are in meters.

For $PR = 2$, a fully supersonic mode of operation is observed. Flow in both isolator and combustor are supersonic. Oblique shock waves generated at the tip of the strut and expansion waves generated at the aft corner of the strut reflect between the top and bottom walls and the shear layers formed between the wake of the strut and the supersonic air streams above and below it. Mach number variations, observed in the flow, result from a combined effect of the variation of flow cross section area, the oblique shocks and the expansion waves through which the flow passes and the state of heat addition due to combustion. The characteristic saw-tooth pattern seen in the pressure profile for the $PR = 2$ reacting case in Fig. 6 can be attributed primarily to these shock and expansion waves through which the flow passes. $PR = 2$ represents a SCRAM mode of operation. For $PR = 7$, also, a fully supersonic mode of operation is observed. Flow in both isolator and combustor are supersonic. In contrast to the $PR = 2$ case, the oblique shockwaves just downstream of the strut are seen to steepen and move upstream towards the base of the strut in response to the increase in static pressure due to increased heat addition. A reduction in the Mach number of the supersonic flow downstream of the shocks is noted. A similar characteristic saw-tooth pattern is seen in the pressure profile, albeit elevated, for the $PR = 7$ reacting case in Fig. 6. For $PR = 10$ a thermally choked transitional mode is observed. For this PR, shockwaves in the combustor move further upstream where they pile near the base of the strut. Downstream of the steepened shock waves, near sonic or choked flow conditions are observed in the air streams above and below the wake of the strut characterised by fine filigree of closely spaced shock waves. Top wall pressure profile for $PR = 10$ in Fig. 6 not only shows a rise in pressure but also a gradual smoothing of the pressure profile, indicating the formation of a subsonic region in the vicinity of the walls. Any further increase in PR causes the flow to switch to RAM mode. For PRs 10.5, 11 and 11.5, the flow field is characterised by the presence of shock waves in the isolator but no oblique shocks at the leading edge of the strut. The flow field in the combustor is predominantly subsonic representing a RAM mode of operation. Top wall pressure for PRs 10.5, 11, 11.5 and 12 in Fig. 6 is accompanied by smoothed pressure profiles in agreement with the presence of subsonic flow. At $PR = 12$, an entirely shock-free, subsonic, mode of operation is observed in the combustor.

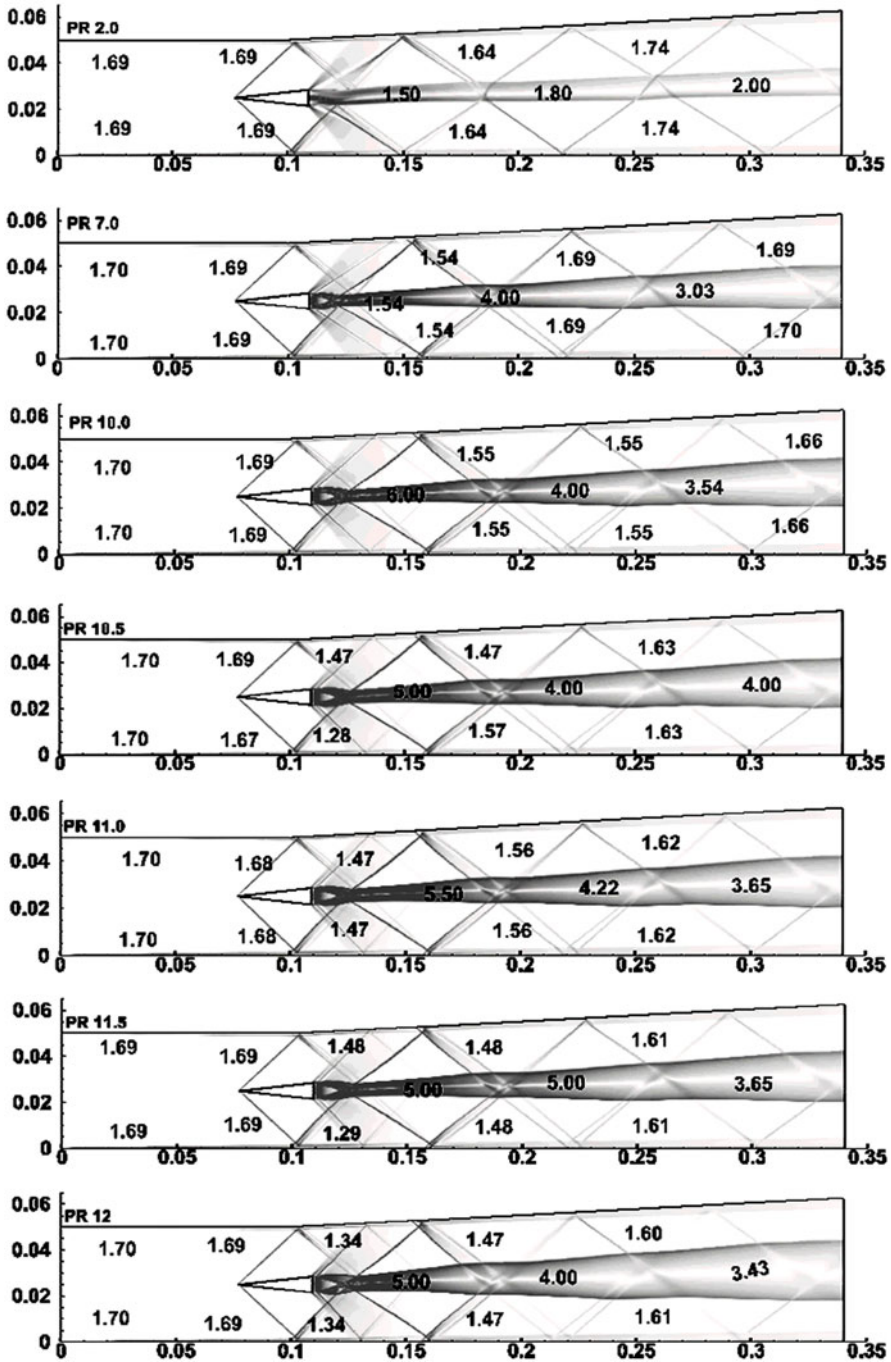


Figure 7. Numerical schlieren for non-reacting cases obtained using RANS for PR = 2, 7, 10, 10.5, 11, 11.5, and 12, respectively, from top to down. Mach numbers superimposed (non-reacting flow).

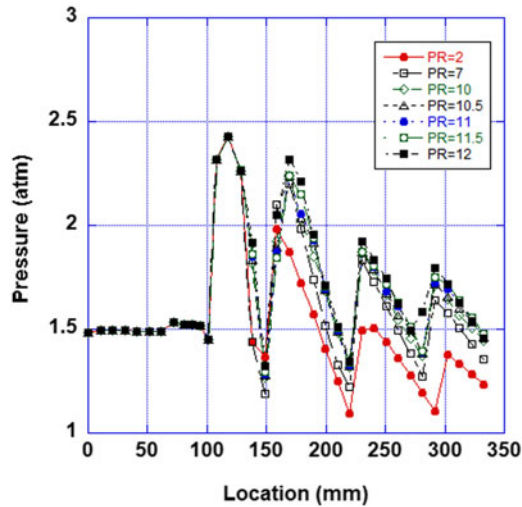


Figure 8. Top wall pressure distribution (non-reacting flow).

In stark contrast to the reacting flow field shown in Fig. 5, Fig. 7 shows flow field for the non-reacting cases for $PR = 2, 7, 10, 10.5, 11, 11.5$ and 12 . A comparison between the reacting and non-reacting flow fields at the same PRs indicate that the shock behaviour in the reacting flow cases is primarily due to the effect of heat addition in the combustor and not due to the effect of fuel mass addition at different PRs alone. The characteristic saw-tooth pattern in the pressure profile for the non-reacting cases shown in Fig. 8 can be attributed to the shock and expansion waves generated due to the strut subsequently reflecting multiple times off the top and bottom walls of the combustor.

The reacting flow fields shown in (Fig. 5) for different PRs may be grouped into two modes (a) Supersonic-at-Strut modes characterised by oblique shock waves anchored at the strut for PRs 2, 7 and 10, and (b) Subsonic-at-Strut modes characterised by shockwaves in the isolator but no oblique shock waves anchored at the strut for PRs 10.5, 11 and 11.5. URANS simulations discussed in Section 4.2 show that the Supersonic-at-Strut modes and the Subsonic-at-Strut modes respond very differently to changes in PR.

4.2 Transient behaviour

URANS (SST $k-\omega$) simulations are used to reveal unsteady behaviour of the shock waves and wall pressure profiles during mode transitions in response to sudden or ramped, increase or decrease in fuel flow rates for different initial and final PRs. For combustor operations at the Supersonic-at-Strut modes, shockwaves in the combustor respond predictably to an increase or decrease in fuel flow rates with intermediate and final flow fields bearing close resemblance to the steady state flow fields predicted by RANS for those fuel flow rates. For combustor operations at the Subsonic-at-Strut modes, an interesting case of instability of the isolator shocks is observed. Any change in fuel flow rate, increase or decrease, sudden or ramped, causes the isolator shocks to immediately move upstream to the upstream end of the isolator.

4.2.1 Supersonic-at-Strut Modes

Figure 9 shows the effect of step increase in PR from 7 to 12. Figure 11 shows the effect of step decrease in PR from 10 to 7. The flow fields, for both the cases, are seen to go through intermediate states bearing resemblance to the RANS predicted flow fields for the intermediate PRs before attaining the RANS

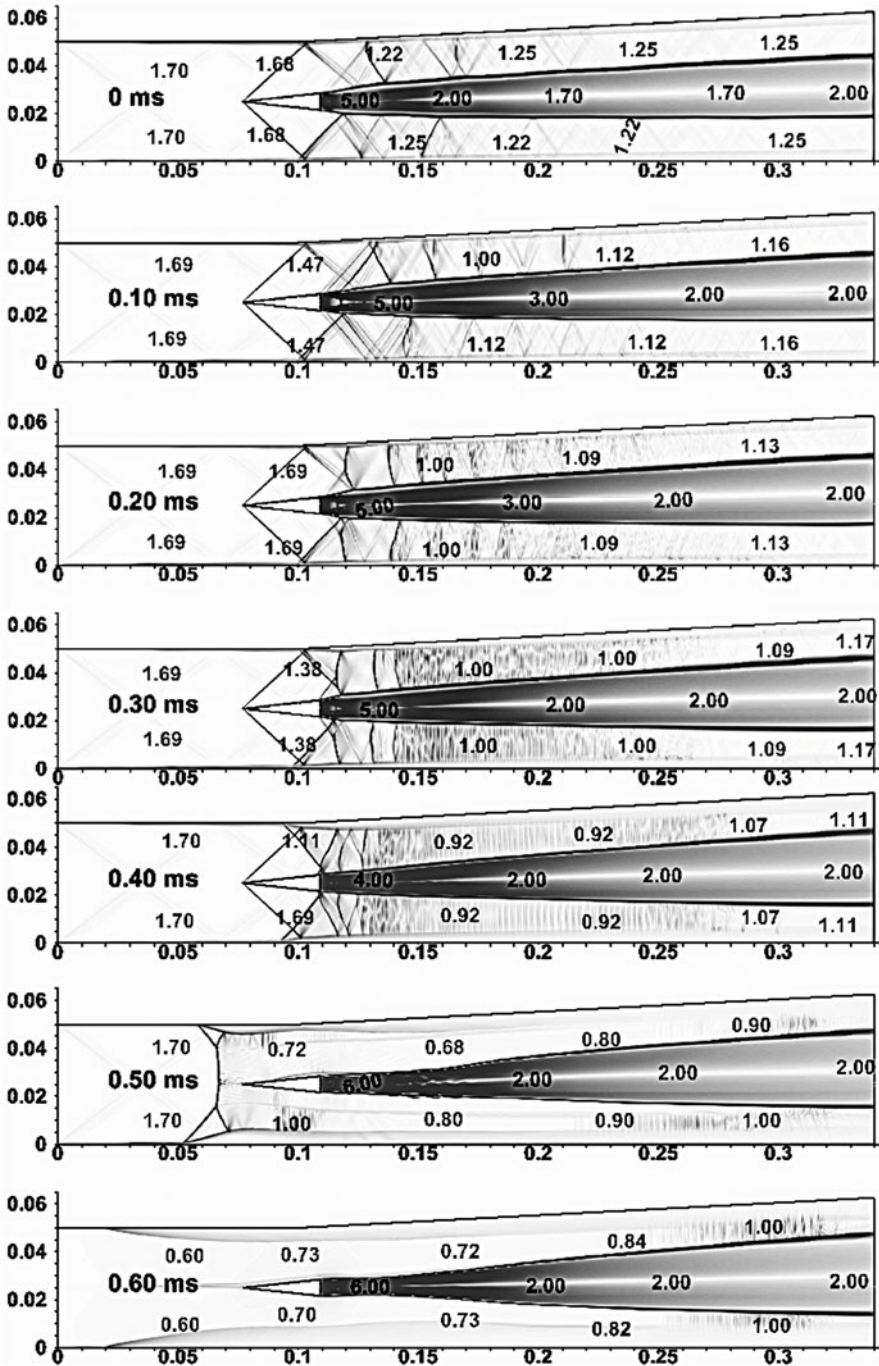


Figure 9. Flow field shown by numerical schlieren images for reacting cases obtained using URANS simulations, for the sudden increase in PR from 7 to 12 (reacting flow).

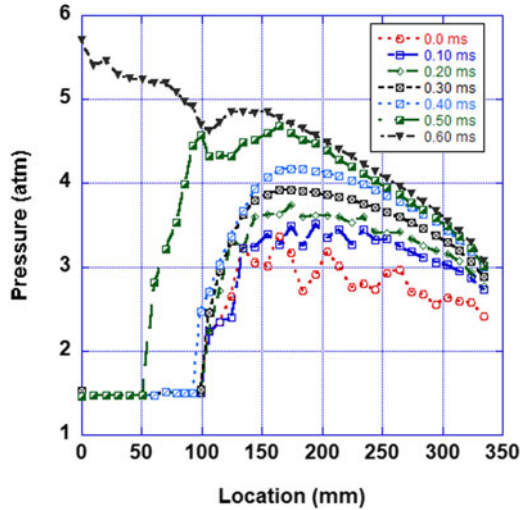


Figure 10. Top wall static pressure due to step increase in PR from 7 to 12 (reacting flow).

predicted flow field at the final PRs. For the PR 7 to PR 12 step increase, oblique shockwaves at the base of the strut for PR = 7 steepen, pile near the base of the strut and eventually move upstream into the isolator. Figure 10 shows the top wall pressure variation during this transition. For the PR 10 to PR 7 step decrease, steepened shockwaves at the base of the strut for PR = 10 spread out and become less steep for PR = 7 to adjust to the reduction in downstream pressure due to a reduction in the amount of heat added. Figure 12 shows pressure data at four different locations—P1, P2, P3 and P4 (shown in Fig. 11) recorded during the step decrease in PR from 10 to 7. Reduction in static pressures at sensor locations P2, P3 and P4 is observed. Location P1, within the isolator, exhibits neither any oscillations nor any reduction in pressure indicating the effectiveness of the isolator in isolating the inlet from pressure variations in the combustor under certain modes of operation. Location P2, near where oblique shock at the strut impinge on the top wall, shows a steady decrease in static pressure leveling off in about 3 ms. Locations P3 and P4, within the combustor, exhibit initial, high frequency, oscillations possibly resulting from upstream transients at the separation shock, the effects of which are convected downstream. The high frequency oscillations at P3, P4 die within about 0.2 ms followed by a gradual reduction in static pressure eventually ending in low amplitude oscillations.

Preliminary tests also show that the transition time in response to an increase in PR bears proportionality to the manner in which the increase in PR is administered. For sudden increase in PR, transitions happen within a millisecond, while for gradual increase in PR, transition time scales with the time through which the PR is ramped. For a sudden increase in PR from 10 to 12, it takes the flow about a millisecond to attain steady state. For a ramped increase of PR from 10 to 12 shown in Fig. 13, the flow takes a timescale commensurate with the ramp time to attain steady state.

Figures 14 and 15 show the complex nature in which the flow-field rearranges itself to accommodate the rise in pressure downstream due to the increase in fuel flow rate when PR is ramped from 10 to 12. Figure 14 shows the intermediate flow-field at 0.05 ms while Fig. 15 shows the intermediate flow-field at 3.0 ms. The large oblique shock at the strut at $t = 0.05$ ms collapses into a small oblique shock at the strut supporting a large lambda shock at $t = 3.0$ ms leading to the generation of multiple slip lines. The lambda-shock at $t = 3.0$ ms supports a higher pressure rise than the oblique shock at $t = 0.05$ ms at the strut followed by a shock train of gradually steepening oblique waves.

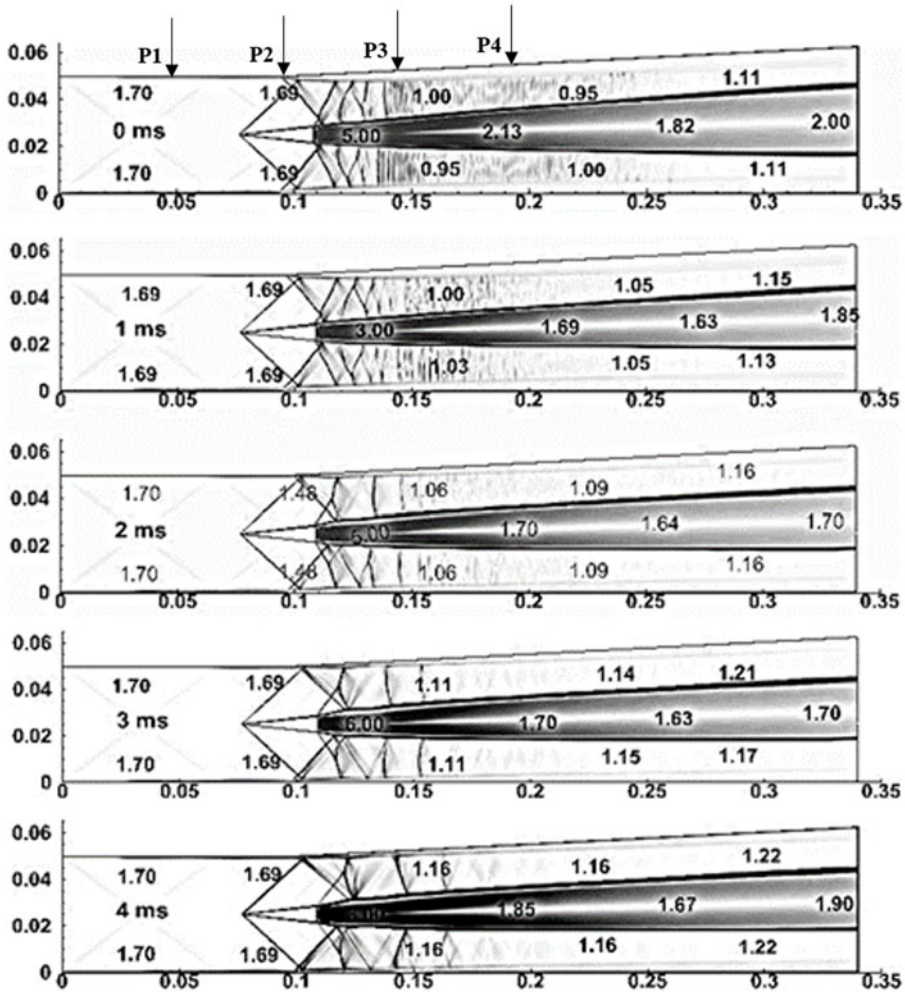


Figure 11. Flow field shown by numerical schlieren images for reacting cases obtained using URANS simulations, for the sudden decrease in PR from 10 to 7 (reacting flow).

4.2.2 Subsonic-at-Strut Modes

For the Subsonic-at-Strut modes of combustion where oblique shocks are absent at the strut (PRs 10.5, 11 and 11.5) but the isolator flow is partly supersonic, the isolator shocks are found to be extremely sensitive to fuel flow rate modulations. Irrespective of the way fuel flow rate is altered, increased or decreased, suddenly or gradually, the shocks in the isolator tend to move upstream immediately rendering the entire flow field within the isolator and the combustor subsonic.

Figures 16 and 17 show the sensitivity of isolator shocks to a sudden and a ramped decrease in PR from 11 to 7, respectively, with both the cases showing similar timescales to reach the steady state flow field from PR = 11 to 7. Figure 18 shows top wall pressure data for step decrease in PR 11 to 7. Tests in which PR is increased from 11 to 11.5 suddenly or through gradual ramping, also show similar behaviour with the isolator shocks moving upstream immediately eventually causing the entire flow field to turn subsonic. Since both increase or decrease in PR, administered suddenly or gradually, causes the isolator shocks to move upstream immediately, it appears some phenomena different from that associated with heat release is responsible for the apparent instability of the isolator shocks to changes in PR.

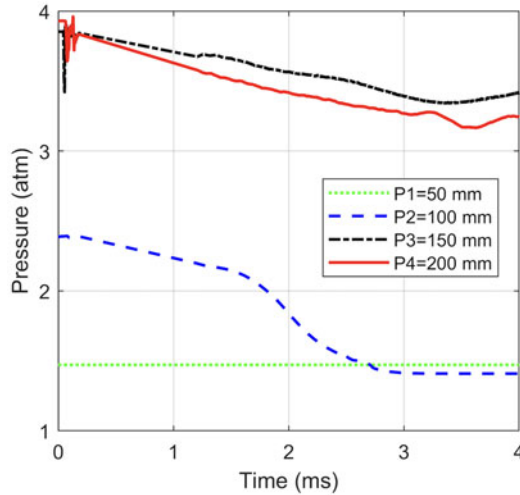


Figure 12. Pressure variation for sudden decrease in PR from 10 to 7.

4.3 Physical mechanism for isolator shock instability

For the Subsonic-at-Strut operating condition, any change in fuel flow rate, sudden or ramped, is seen to cause a characteristic transient undulation of the wake as shown in the inset in Fig. 19 step 1. Given that the sonic throat dd' of a critical streamtube bounded by sliplines formed due to the passage of the supersonic inflow through different regions of the isolator shock is remarkably narrow, any small reduction in the area of the throat, due to such transient undulations of the wake, can cause significant reductions in throat area preventing its ability to pass the mass entering the stream-tube at the supersonic intake. This can result in an accumulation of mass upstream of the throat causing a rise in pressure requiring the isolator shocks to steepen and move upstream. An unstable feedback loop is created in which, as the isolator shocks steepen and move upstream, a greater loss of stagnation pressure in the critical streamtube reduces the ability of the sonic throat to pass mass flow across it further. As a result, the isolator shock system moves upstream, continuously and immediately, the moment fuel flow rate is altered. Although the description of the feedback loop explains the observed flow behaviour, further verification with higher order schemes and carefully controlled experiments will be needed to place this feedback loop among other established critical feedback loops in supersonic engines, such as the one involved in the instability of normal shocks in supersonic flows in convergent ducts [41].

For the Supersonic-at-Strut operating conditions, in contrast, a rise of pressure due to heat addition to a supersonic stream, causes oblique shocks to steepen and eventually pile at the base of the strut. A reduction in PR causes a reduction in the heat added to the supersonic stream causing a decrease in pressure and a reverse behaviour for shocks at the base of the strut is noticed.

5.0 Conclusion

RANS (SST $k-\omega$) simulations are used to obtain steady state behaviour of shock waves and wall pressure profiles under different fuel flow rates for the German Aerospace Center's (DLR), single-strut, parallel-flow DMSJ combustor revealing different modes of combustion under different fuel flow rates. Detailed flow physics of SCRAM, RAM and thermally choked transitional modes obtained under different fuel flow rates are presented. Our work indicates that fuel flow rate, wall pressure data and shockwaves in the flow-field are uniquely mapped to one another, hence given one of the three, the other two can be predicted.

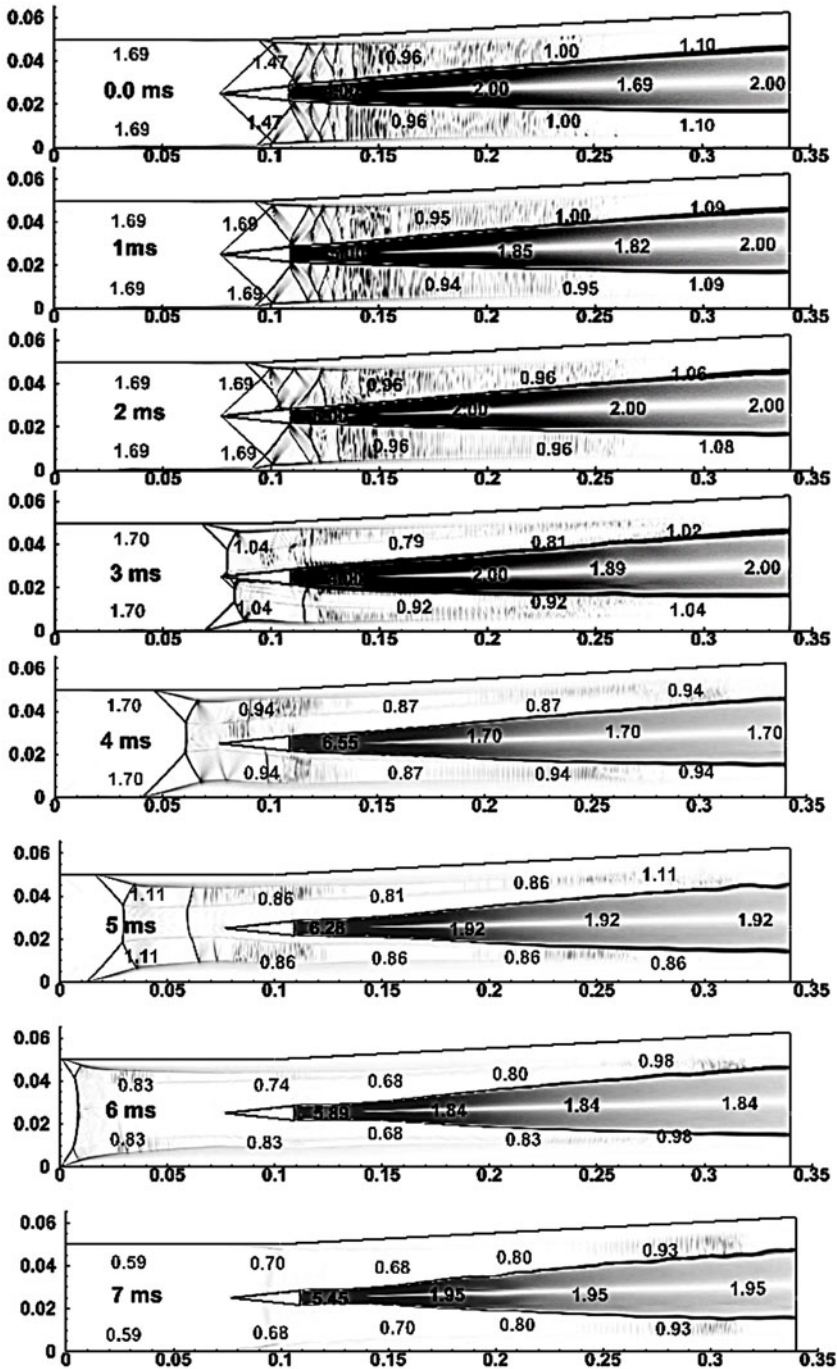


Figure 13. Flow field shown by numerical schlieren images for reacting cases obtained using URANS simulations, for the ramped increase in PR from 10 to 12 (reacting flow).

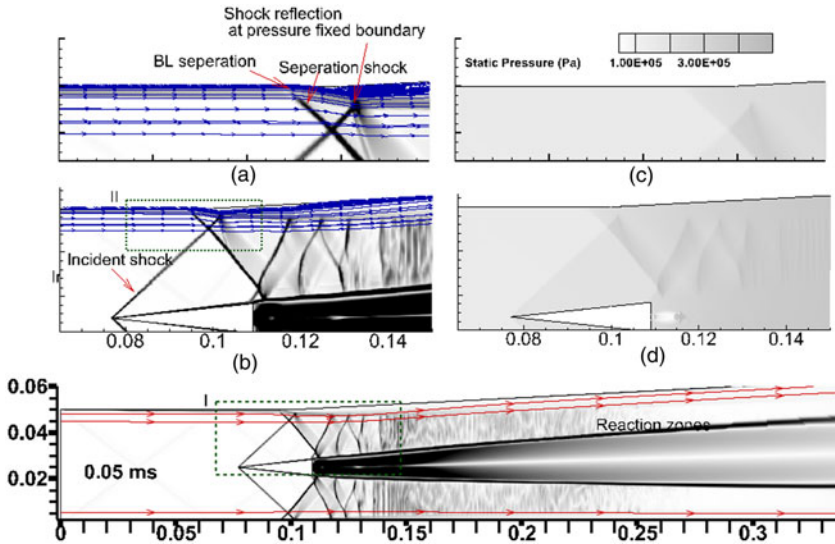


Figure 14. Flow field at 0.05 ms for ramped increase in PR from 10 to 12 (reacting flow).

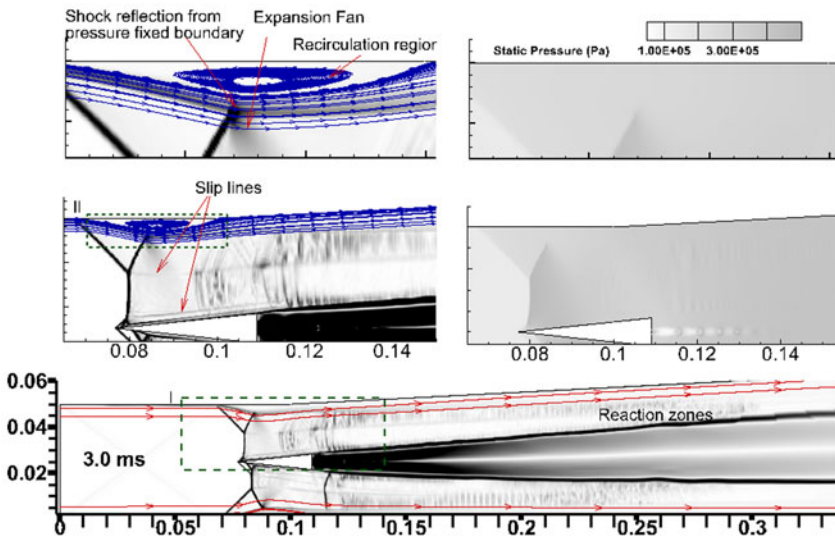


Figure 15. Flow field at 3.0 ms for ramped increase in PR from 10 to 12 (reacting flow).

Two broad modes of operation are identified (a) Supersonic-at-Strut modes characterised by oblique shock waves anchored at the strut for relatively low PRs and (b) Subsonic-at-Strut modes characterised by shockwaves in the isolator but no oblique shock waves anchored at the strut for relatively higher PRs. With the initial condition held either at a Supersonic-at-Strut mode or Subsonic-at-Strut mode, URANS (SST $k-\omega$) simulations are used to reveal unsteady behaviour of the shock waves and wall pressure profiles during mode transitions in response to sudden and ramped, increase or decrease, in fuel flow rates.

For the Supersonic-at-Strut modes, shockwaves in the combustor are shown to respond predictably to an increase or decrease in fuel flow rates. Intermediate and final flow fields bear close resemblance to the steady state flow fields predicted by RANS for those fuel flow rates. Shocks adjust accordingly to

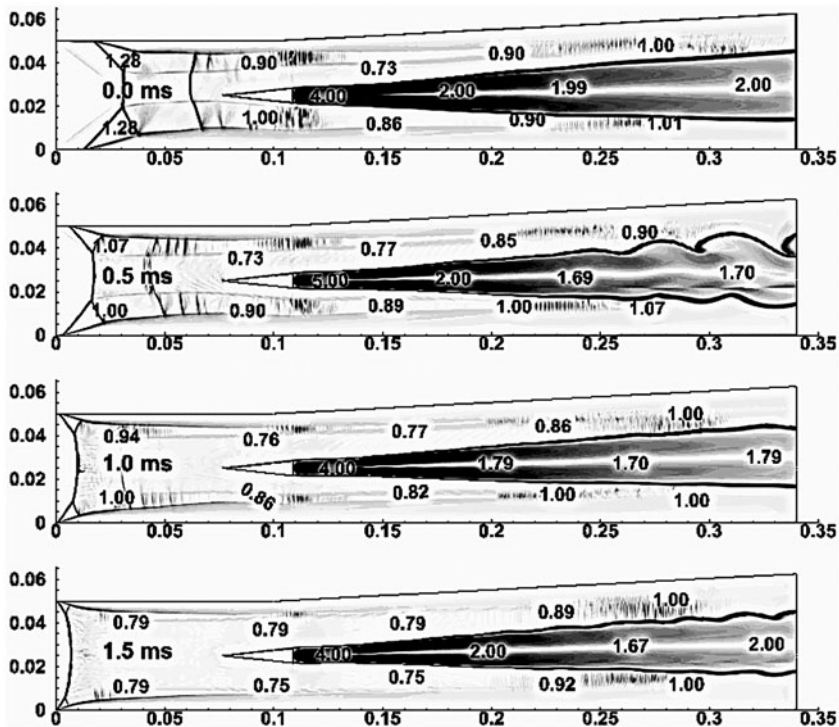


Figure 16. Flow field shown by numerical schlieren images for reacting cases obtained using URANS simulations for the sudden decrease in PR from 11 to 7 (reacting flow).

match the combustion driven pressure rise. Under the Supersonic-at-Strut mode, when fuel flow rate is increased, the shocks steepen and concentrate near the base of the strut. When fuel flow rate is decreased, the opposite trend is observed wherein shocks become more oblique and spread away downstream from the base of the strut.

Feedback control systems that aim at preventing SCRAM-RAM transition could take advantage of the predictable manner in which shockwaves respond to changes in fuel flow rate for the Supersonic-at-Strut modes. The presence of distinct and predictable intermediate markers of transition with respect to shock wave structures and wall pressure profiles allow the possibility of predicting mode transitions and the PRs at which they may occur. The relatively long time through which ramped transitions occur and the short timescale in which a mode can be re-instated through fuel flow rate modulations support the possibility of feedback based control. Since shock waves cannot stabilise on the leading portion of the strut, the detection must be performed while the oblique shock is still anchored at the strut and oblique shock-trains at the base of the strut. While the piling up of shockwaves downstream of the strut can be gradual, shock movements in the leading portion of the strut and in the isolator can be very sudden.

For the Subsonic-at-Strut modes, shockwaves in the flow field are shown to be very unstable to fuel flow rate modulations. Any change in fuel flow rates causes the isolator shocks to immediately move upstream irrespective of if the fuel flow rate is increased or decreased, suddenly or gradually. Because of this instability of isolator shocks for the Subsonic-at-Strut modes, feedback control of isolator shocks using fuel-flow rate modulations alone may not be feasible.

A plausible mechanism for the instability of isolator shocks for the Subsonic-at-Strut modes to fuel flow rate variations is presented. The instability of the isolator shocks to both increase or decrease in fuel flow rate indicates that a mechanism separate from the effect of heat addition to a subsonic stream is operative. For PRs 10.5, 11 and 11.5, when fuel flow rate is modulated, top wall pressure data show rise in

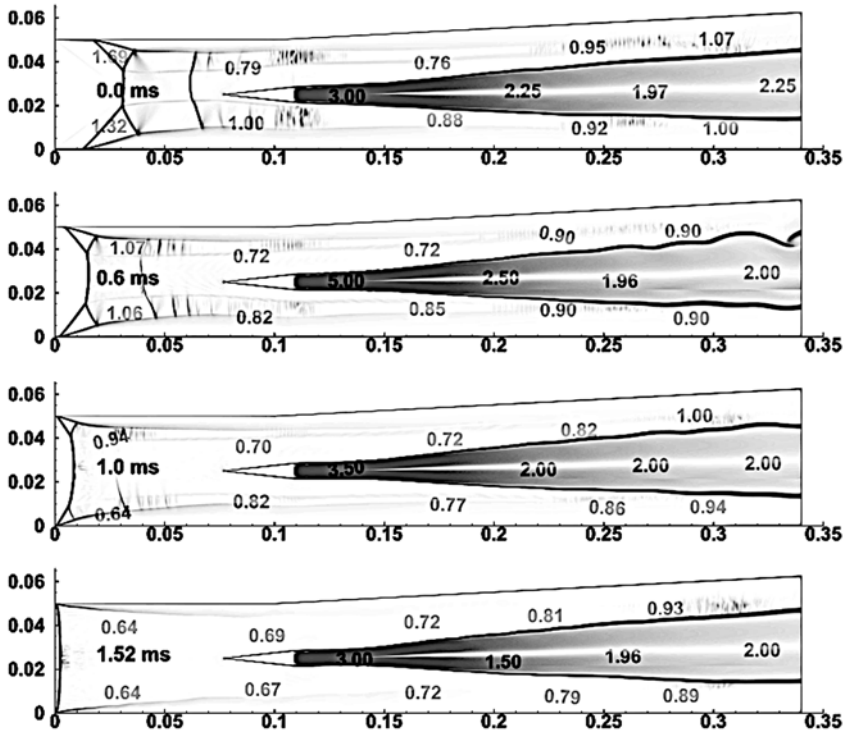


Figure 17. Flow field shown by numerical schlieren images for reacting cases obtained using URANS simulations, ramped decrease in PR from 11 to 7 (reacting flow).

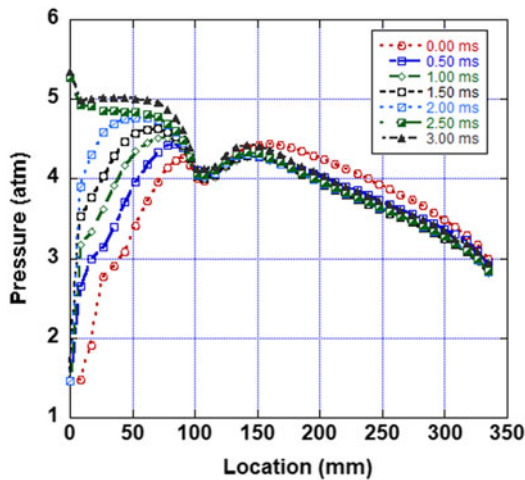


Figure 18. Top wall pressure profile associated with instability of isolator shocks triggered due to step decrease in PR from 11 to 7 (reacting flow).

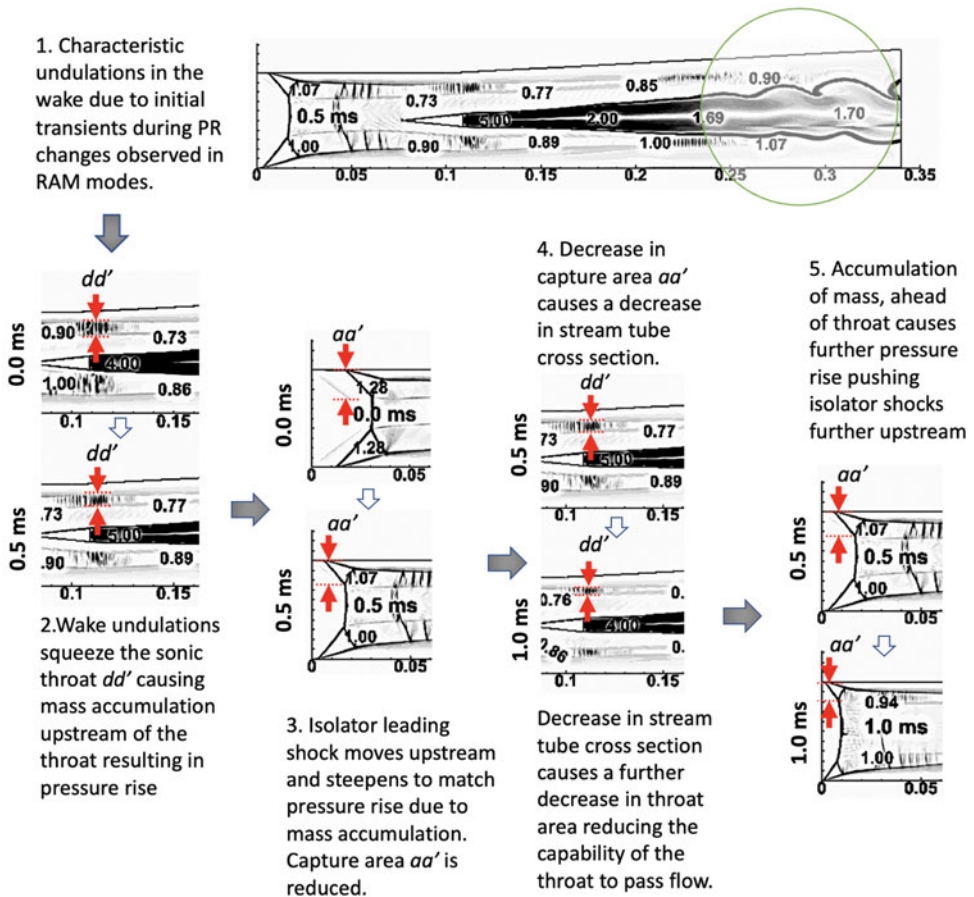


Figure 19. Physical mechanism explaining instability of isolator shock, for a step decrease in PR from 11 to 7 (reacting flow).

pressure upstream of the strut. At the same time, numerical Schlieren data show significant undulations in flame brush thickness at the initiation of the transition. It appears from preliminary tests that the instability of the isolator shocks to fuel flow rate modulations under these PRs could be related to the inability of the choked throat to pass the mass flow in the streamtube due to sudden squeezing action due to the undulations of the flame brush in the wake of the strut. In response to the pressure rise due to accumulation of mass upstream of the contracted sonic throat, the isolator shocks steepen as they move upstream almost immediately, irrespective of if fuel flow is changed abruptly or fuel flow is ramped. While the mechanism is able to explain the observed behaviour in our numerical experiments, the wake mode oscillations on which the mechanism hinges on, needs to be verified with experiments or higher order schemes before the mechanism can be accepted or rejected with a sufficient level of confidence.

For different isolator lengths, the growth of the boundary layer will be different which will affect the pseudo-shock structure. The effect of isolator length has not been explored in this study. Also, a direct connect test has been simulated by forcing boundary conditions at the isolator inlet. The potential phenomenon of inlet unstart due to the movement of shock further upstream out of the inlet has therefore not been possible. The effect of changing Mach number at different PRs on the SCRAM-RAM combustion modes has also not been explored. A future work may address these problems.

Acknowledgements. We acknowledge National Supercomputing Mission (NSM) for providing computing resources of PARAM Shakti at IIT Kharagpur, which is implemented by C-DAC and supported by the Ministry of Electronics and Information Technology (MeitY) and Department of Science and Technology (DST), Government of India. We also acknowledge the support provided by the Science and Engineering Research Board (SERB), Government of India through Grant no. CRG/2022/007335

Declaration of interests. The authors declare that they have no known competing financial interests or personal relationships that could have appeared to influence the work reported in this paper.

References

- [1] Shapiro, A. H, The dynamics and thermodynamics of compressible fluid flow, *New York: Ronald Press*, - 1953.
- [2] Curran, E.T., and Murthy, S.N.B. Scramjet Propulsion, 2001, **189**, AIAA.
- [3] Heiser, W.H., and Pratt, D.T. Hypersonic airbreathing propulsion, 1994, AIAA.
- [4] Cockrell, C. Auslender, A. Guy, R.McClinton, C. and Welch, Sharon Technology roadmap for dual-mode scramjet propulsion to support space-access vision vehicle development, *AIAA/AAAF 11th International Space Planes and Hypersonic Systems and Technologies Conference*, 202, pp 5188.
- [5] Huang, W. Yan, L. and Tan, J. Survey on the mode transition technique in combined cycle propulsion systems, *Aerospace Science and Technology*, Dec 2014, **1**, (39), pp 685-691.
- [6] Kumaran K, Babu V. Investigation of the effect of chemistry models on the numerical predictions of the supersonic combustion of hydrogen. *Combustion and Flame*. 2009 Apr 1; **156** (4):826–41.
- [7] Wang B, Wei W, Ma S and Wei G. Construction of one-step H₂/O₂ reaction mechanism for predicting ignition and its application in simulation of supersonic combustion. *international journal of hydrogen energy*. 2016 Nov 9; **41** (42): 19191–206.
- [8] Billing and Frederick, S., Combustion processes in supersonic flow, *Journal of Propulsion and Power*, 1988, **4**, (3), pp 209-216.
- [9] Sullins, G.A., Demonstration of mode transition in a scramjet combustor, *Journal of Propulsion and Power*, 1993, **9**, (4), pp 515-520.
- [10] Fotia, M.L. Mechanics of combustion mode transition in a direct-connect ramjet scramjet experiment, *Journal of Propulsion and Power*, 2015, **32**, (1), pp 69-78.
- [11] Fotia, M.L. and Driscoll, James. F., Ram-Scram Transition and Flame/Shock-Train Interactions in a Model Scramjet Experiment, *Journal of Propulsion and Power*, Jan 2013, **29**, (1), pp 261-273.
- [12] Fotia, M.L. and Driscoll, James. F., Isolator-combustor interactions in a direct-connect ramjet-scramjet experiment, *Journal of Propulsion and Power*, 2012, **28**, (1), pp 83–95.
- [13] Sun, M.B., Cui, X.D., Wang, H.B., and Bychkov, V. Flame flashback in a supersonic combustor fueled by ethylene with cavity flameholder, *Journal of Propulsion and Power*, 2015, **31**, (3), pp 976–981.
- [14] Kanda, T. Chinzei, N., Kudo, K., and Murakami, A. Dual-Mode Operations in a Scramjet Combustor, *Journal of Propulsion and Power*, Jul 2004, **20**, (4), pp 760-763.
- [15] Kanapathipillai, M., Chang, M., Yu, A., Aguilera, C., and Yu, K. Effect of Distributed Fuel Injection on Model Scramjet Combustor Performance, *AIAA Propulsion and Energy 2020 Forum*, Aug 2020, **31**, (3), pp 976-981.
- [16] Rockwell Jr, R.D., Goyne, C.P., Haw, W., Krauss, R.H., McDaniel, J.C., and Trefny, C.J. Experimental Study of Test-Medium Vitiation Effects on Dual-Mode Scramjet Performance, *Journal of Propulsion and Power*, Sep 2011, **27**, (5), pp 1135-1142.
- [17] Wu, P., Song, W., Wang, Y., and Luo, Y. Estimation of vitiation effects on flameholding and mode transition in a dual-mode supersonic combustor, *Acta Astronautica*, 2021, **185**, pp 117–123.
- [18] O’Byrne, S. Doolan, M., Olsen, S.R., and Houwing, A.F.P. Analysis of Transient Thermal Choking Processes in a Model Scramjet Engine, *Journal of Propulsion and Power*, Sep 2000, **16** (5), pp 808-814.
- [19] Chun, J., Scheuermann, T., von Wolfersdorf, J., and Weigand, B. Experimental Study on Combustion Mode Transition in a Scramjet with Parallel Injection, *14th AIAA/AHI Space Planes and Hypersonic Systems and Technologies Conference*, June 2006.
- [20] Glawe, D.D., Donbar, J.M., Nejad, A.S., Sekar, B., Chen, T.H., Samimy, M., and Driscoll, J.F. Parallel fuel injection from the base of an extended strut into supersonic flow, *32nd Aerospace Sciences Meeting and Exhibit*, Jan 1994.
- [21] Aguilera, C., and Kenneth, H.Y. Effect of Fin-Guided Fuel Injection on Dual Mode Scramjet Operation, *50th AIAA/ASME/SAE/ASEE Joint Propulsion Conference*, Jul 2014.
- [22] Do, H., Passaro, A., and Baccarella, D. Inlet Unstart of an Ethylene-Fueled Model Scramjet with a Mach 4.5 Freestream Flow, *18th AIAA/3AF International Space Planes and Hypersonic Systems and Technologies Conference*, Sep 2012.
- [23] Im, S., Baccarella, D., Olsen, S.R., McGann, B., Liu, Q., Wermer, L., and Do, H. Unstart phenomena induced by mass addition and heat release in a model scramjet, *Journal of Fluid Mechanics*, May 2016, **797**, pp 604-629.
- [24] Liu, Q., Passaro, A., Baccarella, D., and Do, H. Ethylene Flame Dynamics and Inlet Unstart in a Model Scramjet, *American Institute of Aeronautics and Astronautics (AIAA)*, Nov 2014, **30** (6), pp 1577-1585.
- [25] Aguilera, C., and Kenneth, H.Y. Scramjet to ramjet transition in a dual-mode combustor with fin-guided injection, *Proceedings of the Combustion Institute*, Jul 2017 **36** (2), pp 2911-2918.
- [26] Aguilera, C., Ghosh, A., Shin, K.H. and Yu, K.H. Dynamic Pressure Characterization of a Dual-Mode Scramjet, *26th International Colloquium on the Dynamics of Explosions and Reactive Systems (ICDERS)*, July 2017.

- [27] Baccarella, D., Liu, Q., McGann, B., Lee, G., and Lee, T. Isolator-combustor interactions in a circular model scramjet with thermal and non-thermal choking-induced unstart, *Journal of Fluid Mechanics*, Apr 2021, **917**.
- [28] Xue, R., Xu, M., Bai, C., Weng, C., and Xu, C. Study on transient process of mode transition in a scramjet combustor with pilot hydrogen, *International Journal of Energy Research*, Mar 2018, **42** (7), pp 2481–2493.
- [29] Zhang, X., Yue, L., Huang, T., Zhang, Q., and Zhang, X. Numerical investigation of mode transition and hysteresis in a cavity-based dual-mode scramjet combustor, *Aerospace Science and Technology*, Nov 2019, **94**, pp 105420.
- [30] Yan, L., Liao, L., Meng, Y.S., Li, S.B., and Huang, W. Investigation on the mode transition of a typical three-dimensional scramjet combustor equipped with a strut, *Energy*, Oct 2020, **208**, pp 118419.
- [31] Vyas, M., Engblom, W., Georgiadis, N., Trefny, C., and Bhagwandin, V. Numerical Simulation of Vitiation Effects on a Hydrogen-Fueled Dual-Mode Scramjet, *48th AIAA Aerospace Sciences Meeting Including the New Horizons Forum and Aerospace Exposition*, July 2010, pp 1127.
- [32] Kouchi, T., Masuya, G., Mitani, T., and Tomioka, S. Mechanism and Control of Combustion-Mode Transition in a Scramjet Engine, *Journal of Propulsion and Power*, Jan 2012, **28** (1), pp 106-112.
- [33] Michael Oevermann, Numerical investigation of turbulent hydrogen combustion in a SCRAMJET using flamelet modeling, *Aerospace Science and Technology*, Oct 2000, **4** (7), pp 463-480.
- [34] Li, J., Shen, D., Fu, Q., Wang, Y., and Song, W. Mode transition of fuel control test in a dual-mode combustor, *Applied Thermal Engineering*, 2017, **111**, pp 1312–1319.
- [35] Li, J., Jin, R., Jiao, G., and Song, W. Analysis on mode transition in a dual-mode scramjet combustor, *Combustion Science and Technology*, 2018, **190** (1), pp 82–96.
- [36] Tian, Y., Shi, W., Zhong, F., and Le, J. Pilot hydrogen enhanced combustion in an ethylene-fueled scramjet combustor at Mach 4, *Physics of Fluids*, 2021, **33** (1).
- [37] Menter, F.R. Two-equation eddy-viscosity turbulence models for engineering applications, *AIAA Journal*, Aug 1994, **32** (8), pp 1598-1605.
- [38] Choubey, G., Gaud, P., Fatah, A.M., and Devarajan, Y. Numerical investigation on geometric sensitivity and flame stabilisation mechanism in H₂ fueled two-strut based scramjet combustor, *Fuel*, 2022, **312**, pp 122847.
- [39] Kumar, R., Pranaykumar, S., and Ghosh, A. Mode Transition in Cavity Based Dual Mode Scramjet Combustor, *AIAA AVIATION 2023 Forum*, 2023, pp 4138.
- [40] Kumar, R., Iyer, S.G., Prudhvi, N., and Ghosh, A. Mode Transition in a Strut Based Dual-Mode Scramjet Combustor, *AIAA AVIATION 2022 Forum*, 2022, pp 3863.
- [41] Hill, P.G., and Peterson, C.R., *Mechanics and thermodynamics of propulsion*, Reading,- 1992.
- [42] Kouchi, T., Masuya, G., Mitani, T., and Tomioka, S. Mechanism and control of combustion-mode transition in a scramjet engine, *Journal of propulsion and power*, 2012, **28** (1), pp 106–112.